Pergamon

Int. J. Solids Structures Vol. 35, No. 11, pp. 1057–1073, 1998

0020-7683/98 $19.00 + .00

PII: S0020-7683(97)00108-X

STRESS SINGULARITIES IN ANISOTROPIC MULTI-MATERIAL WEDGES AND JUNCTIONS

HUA-PENG CHEN†
Department of Civil Engineering, Imperial College of Science, Technology and Medicine, London, SW7 2BU, U.K.

(*Received* 3 *September* 1996; *in revised form* 4 *March* 1997)

Abstract—The general problem of stress singularities in anisotropic multi-material wedges and junctions due to geometric and material discontinuities is investigated. The anisotropic wedges and junctions discussed here comprise two or three materials with different geometric configurations and different material properties. The interfaces in multi-material junctions are either all perfectly bonded or a disbond is introduced along one interface. The order of stress singularities is obtained by solving the characteristic equations that are developed from the boundary conditions of the problem. Numerical examples for the order of stress singularities are given for the general problem including two and three-material wedges, a crack terminating at an interface between two materials, bonded and disbonded two and three-material junctions as well. An "extra" root of the characteristic equations in addition to three roots corresponding to higher singular stresses is observed for the cases of disbonded anisotropic two and three-material junctions. The stress singularities affected by geometric configurations and material properties of anisotropic materials are also investigated.
© 1998 Elsevier Science Ltd.

1. INTRODUCTION

The stress singularity can exist in anisotropic elastic solids when discontinuities are present in the geometry and/or the material properties of the materials, such as anisotropic multi-material wedges, bonded and disbonded multi-material junctions. Some problems considered in this paper are shown in Fig. 1 in which one disbond may be introduced along an interface in multi-material junctions. The points that are internal to the body and labelled o as shown in Figs 1(a), (b) and (c) are the locations of the stress singularities.

The stress singularities for bonded and disbonded isotropic three-material junctions have been investigated by Pageau *et al.* (1994) and Inoue *et al.* (1996). The stress singularities for several special configurations of anisotropic materials, such as free edge in laminated composites, bonded anisotropic wedges and anisotropic layered composites with a crack normal to an interface, has been studied by Ting *et al.* (1981, 1984), Delale (1984) and Huang *et al.* (1994). In addition, Wang *et al.* (1982) analysed boundary layer stress singularities in composite laminates under uniform extension using Lekhnitskii's stress potentials (Lekhnitskii, 1963). Zwiers *et al.* (1982) utilised the Stroh's formulation (Stroh, 1962) to study the same problem. A logarithmic singularity of free-edge may exist in addition to the same power singularity as obtained by Wang *et al.* (1982). Yeh (1986) presented a finite element formulation based on singularity transformation. An approximate order of stress singularity at the boundary layer of an interface between adjacent anisotropic layers was obtained. Recently, Pageau *et al.* (1996) developed a finite element approach to analyse three-dimensional singular stress states in prismatic configurations of anisotropic multi-material wedges and junctions. A more general three-dimensional finite element analysis of singularities where multi-material junctions intersect free surfaces has also been presented by Pageau *et al.* (1995).

In this paper, the general problem of stress singularities in anisotropic multi-material composites, such as two and three-material wedges, bonded and disbonded two and three-material junctions, is considered. The geometry for the general problem of an anisotropic

† Previously worked at Dept of Civil Engineering, Ningbo University, Zhejiang, China. Present address for correspondence: Dept of Civil Engineering, The University of Glasgow, Glasgow G12 8LT, U.K. E-mail: hchen@civil.gla.ac.uk

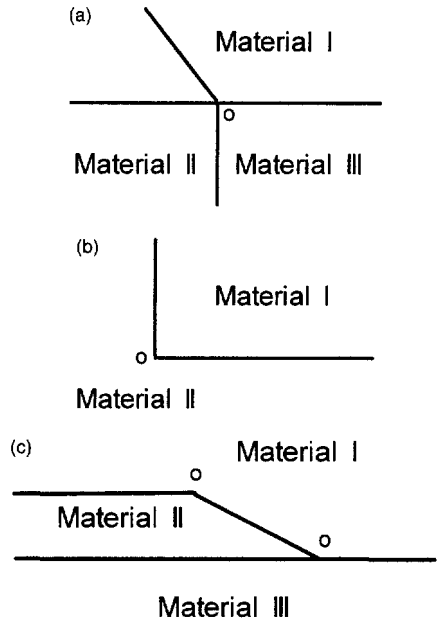

Fig. 1. Examples of multi-material wedges and junctions. (a) Three material wedge. (b) Two material junction. (c) Three material junction.

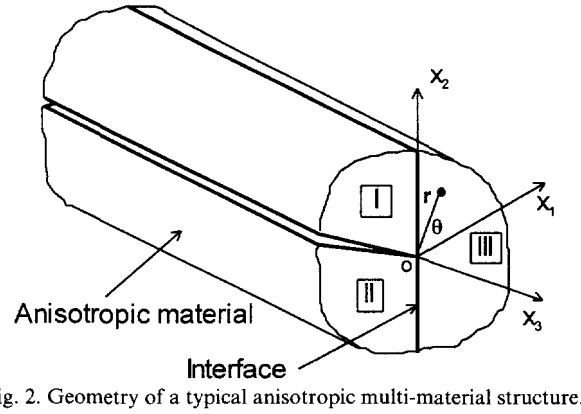

Fig. 2. Geometry of a typical anisotropic multi-material structure.

multi-material junction is shown in Fig. 2, where wedge and junction configurations are considered as prisms in the direction along the line of singular point, i.e., along the x_3 direction. Each anisotropic material is a fibre reinforced composite in which the fibres are assumed to lie in x_2-x_3 plane although the proposed method is not limited to these cases. The orientations of the fibres may vary from material to material and are measured from the x_2-axis by the angle α_I, α_{II} and α_{III} for material I, II and III, respectively. Based on the displacements and stresses near the tip of an interface crack in anisotropic composites developed by Ting (1986) using Stroh's formulation, the characteristic equations for the cases of anisotropic multi-material wedges and junctions are established. The order of stress singularities for these cases is obtained by solving the corresponding characteristic equations. Finally, the stress singularities affected by the geometric configurations, e.g., the wedge angle, the crack position, the bonded interface position and the disbond position, and material properties, e.g. the fibre orientation, are investigated.

2. FORMULATION

The equations for the displacements and stresses at the tip of an interface crack in an anisotropic composite were developed by Ting (1986) where a two-dimensional deformation

in which displacements depend on x_1 and x_2 only is considered. The displacement vector **u** and the surface traction vector **t** on the polar plane (r, θ) near the vertex of an anisotropic wedge used here and after can be expressed as follows

$$u(\theta) = \sum_{\omega=1}^{3} (q_\omega a_\omega z_\omega^{\delta+1} + h_\omega \bar{a}_\omega \bar{z}_\omega^{\delta+1})/(\delta+1) \tag{1}$$

$$t(\theta) = \sum_{\omega=1}^{3} \frac{1}{r}(q_\omega b_\omega z_\omega^{\delta+1} + h_\omega \bar{b}_\omega \bar{z}_\omega^{\delta+1}) \tag{2}$$

where

$$z_\omega = x_1 + p_\omega x_2 = r(\cos\theta + p_\omega \sin\theta) \tag{3}$$

in which q_ω and h_ω are arbitrary constants; p_ω and $\{\mathbf{a}_\omega, \mathbf{b}_\omega\}^T$ as well as their complex conjugates are the eigenvalues and eigenvectors determined by the elasticity constants; an over bar denotes the complex conjugate. In this paper, the formulation is extended to be used for the general problem of anisotropic multi-material wedges and junctions.

Equations (1) and (2) can be rewritten in the following matrix form

$$u(\theta) = r^{\delta+1}\{AE(\delta,\theta)q + \bar{A}\hat{E}(\delta,\theta)h\}/(\delta+1) \tag{4}$$

$$t(\theta) = r^{\delta}\{BE(\delta,\theta)q + \bar{B}\hat{E}(\delta,\theta)h\} \tag{5}$$

where vectors **q** and **h** comprise arbitrary constants q_ω and h_ω, respectively; matrix **A** and **B** comprise vectors $\mathbf{a}_\omega$ and $\mathbf{b}_\omega$, respectively; and diagonal matrices $E(\delta, \theta)$ and $\hat{E}(\delta, \theta)$ are defined as

$$E(\delta,\theta) = \mathrm{Diag}[\eta_1^{\delta+1}, \eta_2^{\delta+1}, \eta_3^{\delta+1}] \tag{6}$$

$$\hat{E}(\delta,\theta) = \mathrm{Diag}[\bar{\eta}_1^{\delta+1}, \bar{\eta}_2^{\delta+1}, \bar{\eta}_3^{\delta+1}] \tag{7}$$

in which

$$\eta_\omega = \cos\theta + p_\omega \sin\theta, \omega = 1,3. \tag{8}$$

Since the surface traction vector **t** is of the order r^δ, the stresses are singular if the real part of δ is negative.

Consider now the boundary conditions for the general problem. The traction-free boundary conditions on the radical surface $\theta = \phi$ are

$$t(\phi) = 0 \tag{9}$$

and the continuity conditions for fully bonded interface between material I and material II on the radical surface $\theta = \phi$ are

$$u_{\mathrm{I}}(\phi) - u_{\mathrm{II}}(\phi) = 0 \tag{10a}$$

$$t_{\mathrm{I}}(\phi) - t_{\mathrm{II}}(\phi) = 0. \tag{10b}$$

Based on the displacement vector **u** and the surface traction vector **t** in eqns (4) and (5), the characteristic equations for the following cases can be established using the combinations of boundary conditions discussed above.

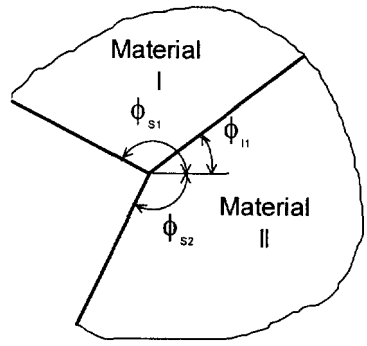

Fig. 3. Geometry for the problem of a two-material wedge.

2.1. *Characteristic equations for two-material wedges and junctions*

Wedges. Consider a two-material wedge that is perfectly bonded along the interface $\theta = \phi_{I1}$ as shown in Fig. 3. The surfaces of material I $\theta = \phi_{S1}$ and material II $\theta = \phi_{S2}$ are assumed to be traction free. Application of eqns (9) and (10) leads to the following characteristic equations

$$B_I E_I(\delta, \phi_{S1}) q_I + \bar{B}_I \hat{E}_I(\delta, \phi_{S1}) h_I = 0 \tag{11a}$$

$$B_{II} E_{II}(\delta, \phi_{S2}) q_{II} + \bar{B}_{II} \hat{E}_{II}(\delta, \phi_{S2}) h_{II} = 0 \tag{11b}$$

$$A_I E_I(\delta, \phi_{I1}) q_I + \bar{A}_I \hat{E}_I(\delta, \phi_{I1}) h_I - A_{II} E_{II}(\delta, \phi_{I1}) q_{II} - \bar{A}_{II} \hat{E}_{II}(\delta, \phi_{I1}) h_{II} = 0 \tag{11c}$$

$$B_I E_I(\delta, \phi_{I1}) q_I + \bar{B}_I \hat{E}_I(\delta, \phi_{I1}) h_I - B_{II} E_{II}(\delta, \phi_{I1}) q_{II} - \bar{B}_{II} \hat{E}_{II}(\delta, \phi_{I1}) h_{II} = 0 \tag{11d}$$

Fully bonded junctions. When the surfaces of material I $\theta = \phi_{S1}$ and material II $\theta = \phi_{S2}$ shown in Fig. 3 are perfectly bonded together, the problem of Fig. 3 becomes the one of a fully bonded junction with two interfaces between two materials, i.e., $\theta = \phi_{I1}$ and $\theta = \phi_{I2}$. Therefore, the characteristic equations can be written as equations (11c, d) plus eqns (12a, b)

$$A_I E_I(\delta, \phi_{I2}) q_I + \bar{A}_I \hat{E}_I(\delta, \phi_{I2}) h_I - A_{II} E_{II}(\delta, \phi_{I2}) q_{II} - \bar{A}_{II} \hat{E}_{II}(\delta, \phi_{I2}) h_{II} = 0 \tag{12a}$$

$$B_I E_I(\delta, \phi_{I2}) q_I + \bar{B}_I \hat{E}_I(\delta, \phi_{I2}) h_I - B_{II} E_{II}(\delta, \phi_{I2}) q_{II} - \bar{B}_{II} \hat{E}_{II}(\delta, \phi_{I2}) h_{II} = 0. \tag{12b}$$

Disbonded junctions. The case of a disbonded two-material junction can be obtained when the surfaces of material I and material II shown in Fig. 3 are located on the radical surfaces $\theta = \phi_{S1}$ and $\theta = \phi_{S2} = -2\pi + \phi_{S1}$, respectively. The characteristic equations for this case are the same as those for two-material wedge, eqn (11), in which ϕ_{S2} in eqn (11b) is considered as $\phi_{S2} = -2\pi + \phi_{S1}$.

Note that the characteristic equations for all three cases mentioned above comprise a set of total 12 equations.

Crack terminating at an interface. The geometry for this case is shown in Fig. 4. Two materials are perfectly bonded on the radical surfaces $\theta = \phi_{I1}$ and $\theta = \phi_{I2}$, and a crack is

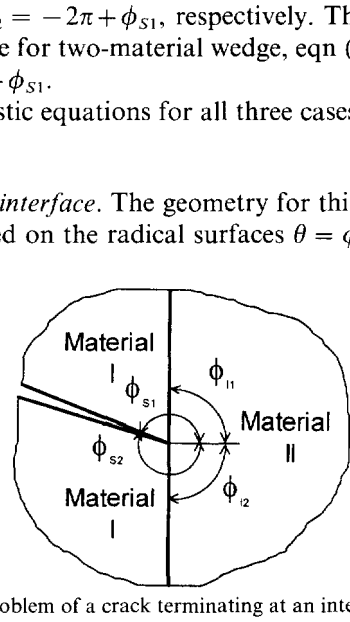

Fig. 4. Geometry for the problem of a crack terminating at an interface between two materials.

present in material I with free crack surfaces $\theta = \phi_{S1}$ and $\theta = \phi_{S2} = -2\pi + \phi_{S1}$. The characteristic equations for this problem are written as follows

$$B_I E_I(\delta, \phi_{S1}) q_{II} + \bar{B}_I \hat{E}_I(\delta, \phi_{S1}) h_{II} = 0 \tag{13a}$$

$$B_I E_I(\delta, \phi_{S2}) q_{I2} + \bar{B}_I \hat{E}_I(\delta, \phi_{S2}) h_{I2} = 0 \tag{13b}$$

$$A_I E_I(\delta, \phi_{II}) q_{II} + \bar{A}_I \hat{E}_I(\delta, \phi_{II}) h_{II} - A_{II} E_{II}(\delta, \phi_{II}) q_{II} - \bar{A}_{II} \hat{E}_{II}(\delta, \phi_{II}) h_{II} = 0 \tag{13c}$$

$$B_I E_I(\delta, \phi_{II}) q_{II} + \bar{B}_I \hat{E}_I(\delta, \phi_{II}) h_{II} - B_{II} E_{II}(\delta, \phi_{II}) q_{II} - \bar{B}_{II} \hat{E}_{II}(\delta, \phi_{II}) h_{II} = 0 \tag{13d}$$

$$A_I E_I(\delta, \phi_{I2}) q_{I2} + \bar{A}_I \hat{E}_I(\delta, \phi_{I2}) h_{I2} - A_{II} E_{II}(\delta, \phi_{I2}) q_{II} - \bar{A}_{II} \hat{E}_{II}(\delta, \phi_{I2}) h_{II} = 0 \tag{13e}$$

$$B_I E_I(\delta, \phi_{I2}) q_{I2} + \bar{B}_I \hat{E}_I(\delta, \phi_{I2}) h_{I2} - B_{II} E_{II}(\delta, \phi_{I2}) q_{II} - \bar{B}_{II} \hat{E}_{II}(\delta, \phi_{I2}) h_{II} = 0. \tag{13f}$$

Here, the characteristic eqn (13) comprises at set of total 18 equations.

2.2. *Characteristic equations for three-material wedges and junctions*

Wedges. The geometry of a three-material wedge is shown in Fig. 5. Three materials are perfectly bonded at two interfaces, i.e., interface $\theta = \phi_{I1}$ between material I and material III, and interface $\theta = \phi_{I2}$ between material II and material III. The surfaces of material I $\theta = \phi_{S1}$ and material II $\theta = \phi_{S2}$ are assumed to be traction free. Application of these boundary conditions yields the following characteristic equations

$$B_I E_I(\delta, \phi_{S1}) q_I + \bar{B}_I \hat{E}_I(\delta, \phi_{S1}) h_I = 0 \tag{14a}$$

$$B_{II} E_{II}(\delta, \phi_{S2}) q_{II} + \bar{B}_{II} \hat{E}_{II}(\delta, \phi_{S2}) h_{II} = 0 \tag{14b}$$

$$A_I E_I(\delta, \phi_{I1}) q_I + \bar{A}_I \hat{E}_I(\delta, \phi_{I1}) h_I - A_{III} E_{III}(\delta, \phi_{I1}) q_{III} - \bar{A}_{III} \hat{E}_{III}(\delta, \phi_{I1}) h_{III} = 0 \tag{14c}$$

$$B_I E_I(\delta, \phi_{I1}) q_I + \bar{B}_I \hat{E}_I(\delta, \phi_{I1}) h_I - B_{III} E_{III}(\delta, \phi_{I1}) q_{III} - \bar{B}_{III} \hat{E}_{III}(\delta, \phi_{I1}) h_{III} = 0 \tag{14d}$$

$$A_{II} E_{II}(\delta, \phi_{I2}) q_{II} + \bar{A}_{II} \hat{E}_{II}(\delta, \phi_{I2}) h_{II} - A_{III} E_{III}(\delta, \phi_{I2}) q_{III} - \bar{A}_{III} \hat{E}_{III}(\delta, \phi_{I2}) h_{III} = 0 \tag{14e}$$

$$B_{II} E_{II}(\delta, \phi_{I2}) q_{II} + \bar{B}_{II} \hat{E}_{II}(\delta, \phi_{I2}) h_{II} - B_{III} E_{III}(\delta, \phi_{I2}) q_{III} - \bar{B}_{III} \hat{E}_{III}(\delta, \phi_{I2}) h_{III} = 0. \tag{14f}$$

Fully bonded junctions. When the surfaces of material I $\theta = \phi_{S1}$ and material II $\theta = \phi_{S2}$ shown in Fig. 5 are perfectly bonded together, the case of three-material wedge of Fig. 5 becomes the one of a fully bonded three-material junction with three bonded interfaces, i.e., $\theta = \phi_{I1}$, $\theta = \phi_{I2}$ and $\theta = \phi_{I3}$. Therefore, the characteristic equations for this problem can be expressed as the eqns (14c–f) for two bonded interfaces $\theta = \phi_{I1}$ and $\theta = \phi_{I2}$ plus the eqns (15a, b) for the new bonded interface $\theta = \phi_{I3}$ between material I and material II

$$A_I E_I(\delta, \phi_{I3}) q_I + \bar{A}_I \hat{E}_I(\delta, \phi_{I3}) h_I - A_{II} E_{II}(\delta, \phi_{I3}) q_{II} - \bar{A}_{II} \hat{E}_{II}(\delta, \phi_{I3}) h_{II} = 0 \tag{15a}$$

$$B_I E_I(\delta, \phi_{I3}) q_I + \bar{B}_I \hat{E}_I(\delta, \phi_{I3}) h_I - B_{II} E_{II}(\delta, \phi_{I3}) q_{II} - \bar{B}_{II} \hat{E}_{II}(\delta, \phi_{I3}) h_{II} = 0. \tag{15b}$$

Disbonded junctions. The case of a disbonded three-material junction can be obtained from the case of a three-material fully bonded junction when a disbond is introduced along

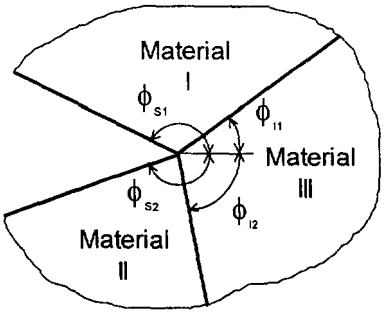

Fig. 5. Geometry for the problem of a three-material wedge.

any one interface. The characteristic equations for the case of a disbonded three-material junction with a disbond along the interface between material I and material II are the same as those for a three-material wedge, characteristic eqn (14), in which ϕ_{S2} in eqn (14b) is considered as $\phi_{S2} = -2\pi + \phi_{S1}$. The characteristic equations for the cases of three-material junctions with a disbond along any one of other interfaces can be also obtained by the same method as indicated above.

Note that the characteristic equations comprise a set of total 18 equations for all cases of three-material wedges, bonded and disbonded three-material junctions.

The characteristic equations developed here for each case constitute a system of homogeneous linear algebraic equations in arbitrary coefficients **q** and **h**. The existence of a nontrivial solution for **q** and **h** requires vanishing of the coefficient determinant

$$|\Delta(\delta)| = 0 \tag{16}$$

where $\Delta(\delta)$ is a coefficient matrix involving δ. The results for eqn (16) can be obtained using standard numerical techniques such as Muller's method (Muller, 1956).

3. NUMERICAL RESULTS

Two different illustrative composite materials are utilised for the numerical calculations in order to compare the present results with the existing results. The engineering constants for the layers in the two composites are taken from Delale (1984) and Wang *et al.* (1977), respectively.

$$\begin{aligned} &E_L = 163.4 \times 10^6\, kPa, E_T = E_Z = 11.9 \times 10^6\, kPa \\ &G_{LT} = G_{ZL} = 6.5 \times 10^6\, kPa, G_{ZT} = 3.5 \times 10^6\, kPa \\ &\nu_{LT} = \nu_{LZ} = 0.3, \nu_{TZ} = 0.5 \end{aligned} \tag{17}$$

and

$$\begin{aligned} &E_L = 137.90 \times 10^6\, kPa, E_T = E_Z = 14.48 \times 10^6\, kPa \\ &G_{LT} = G_{LZ} = G_{TZ} = 4.98 \times 10^6\, kPa \\ &\nu_{LT} = \nu_{LZ} = \nu_{TZ} = 0.21 \end{aligned} \tag{18}$$

where E, G and ν are the Young's modulus, shear modulus and Possion's ratio, respectively. The subscripts L, T and Z refer to the fibre, transverse and thickness directions of an individual layer, respectively. The fibre orientations measured from the x_2-axis by the angle α are assumed to differ from layer to layer. Equation (17) is used for the calculations of the problems of two-material wedges, bonded and disbonded two-material junctions (see Figs 6–11), while eqn (18) is used for the calculations of the problems of a crack terminating an interface between two materials, three-material wedges, bonded and disbonded three-material junctions (see Figs 12–21).

In order to show the effects of geometric configurations and material properties on the stress singularity, various numerical examples for multi-material wedges, bonded and disbonded multi-material junctions are discussed here. The order of stress singularity for each case is determined from the corresponding characteristic equations when the real part of root δ is negative. Both real and complex roots may be found for some cases. Since complex conjugates of these values are also roots of the characteristic equations, only positive imaginary parts of complex roots are considered. In the following figures, the real parts of complex roots, Re δ, are represented by solid lines, while the imaginary parts of complex roots, Im δ, are represented by broken lines.

The comparison between the selected present results and the existing results is given for some special cases of geometric configurations and fibre orientations discussed here as

Table 1. Values of roots for special cases of multi-material wedges and junctions compared to the existing results

Figure	Geometry configuration θ	Fibre orientation α	Current value	Existing value	Ref.*
Fig. 6		$\alpha = 60°$	-0.422886	-0.4229	[1]
Fig. 7	$\theta = 90°$		-0.380828		
			-0.047337		
Fig. 7	$\theta = 179°$		-0.499479	-0.4995	[1]
			$-0.498481 \pm 0.019609i$		
Fig. 12		$\alpha = 30°$	-0.662510	-0.663106	[2]
Fig. 13	$\theta = 180°$		-0.494838	-0.494451	
			-0.347946	-0.348117	
Fig. 13	$\theta = 90°$		-0.500000	-0.5008	[3]
	$\theta = 270°$		$-0.500000 \pm 0.029421i$	$-0.4992 \pm 0.0291i$	
Fig. 16		$\alpha = 45°$	-0.082543	-0.084240	[2]
Fig. 17	$\theta = 180°$		-0.018759	-0.019218	
Fig. 18		$\alpha = 45°$	-0.614880	-0.615097	[2]
Fig. 21	$\theta = 180°$		-0.490522	-0.490090	
			-0.385132	-0.385501	
			-0.004092		
Fig. 19		$\alpha = 45°$	-0.585143	N/A	N/A
Fig. 20		$\alpha = 0°$	-0.504003		
			-0.455394		
			-0.009197		

* Ref.: [1] Delale (1984). [2] Pegeau *et al.* (1996). [3] Yeh *et al.* (1986).

summarised in Table 1. Only first few roots that correspond to higher singular stresses are available in the existing results. However, all of roots that correspond to singular stresses are obtained using the proposed method, and the values of roots are more accurate compared with the results obtained by finite element approach. Here, an "extra" root that corresponds to very low singular stresses is found in the cases of Figs 18–21 as listed in Table 1, which is prone to be neglected using finite element approach. To the author's knowledge, four roots, including the "extra" one, that correspond to singular stresses in anisotropic multi-material wedges and junctions have not been found previously.

3.1. *Results for two-material wedges and junctions*

Wedges. The influence of wedge angles and material properties for two-material wedges on the stress singularity is investigated. The results in Fig. 6 are for the case of a two-material wedge with a 90° wedge angle for material I and a half plane for material II. The fibre orientation of material I is variable, i.e., $\alpha_I = \alpha$ where α varies from $-90°$ to 90°, while the fibre orientation of material II is fixed, $\alpha_{II} = 30°$. The order of stress singularity varying with α_I is also shown in Fig. 6. Three real roots that correspond to singular stresses exist for the full variation range of fibre orientations of material I α_I. The values of roots δ are identical for the cases of $\alpha_I = -90°$ and $\alpha_I = 90°$, where both fibre orientations for material I are the same.

Figure 7 shows the case of a two-material wedge with fixed fibre orientations for material I $\alpha_I = 60°$ and material II $\alpha_{II} = 30°$, while the wedge angle for material I θ varies from 0° to 180°. The effect of the wedge angle θ on the stress singularity is investigated as shown in Fig. 7. From the results, it can be seen that the stress singularity becomes more severe as the wedge angle θ increases, reaching the value of a real root $-1/2$ and a pair of complex conjugate roots with real parts $-1/2$ for an interface crack between two anisotropic materials. In addition, two real roots exist for wedge angle θ ranging from 0° to near 90°, and a real root together with a pair of complex conjugate roots is present for wedge angle θ near 180°.

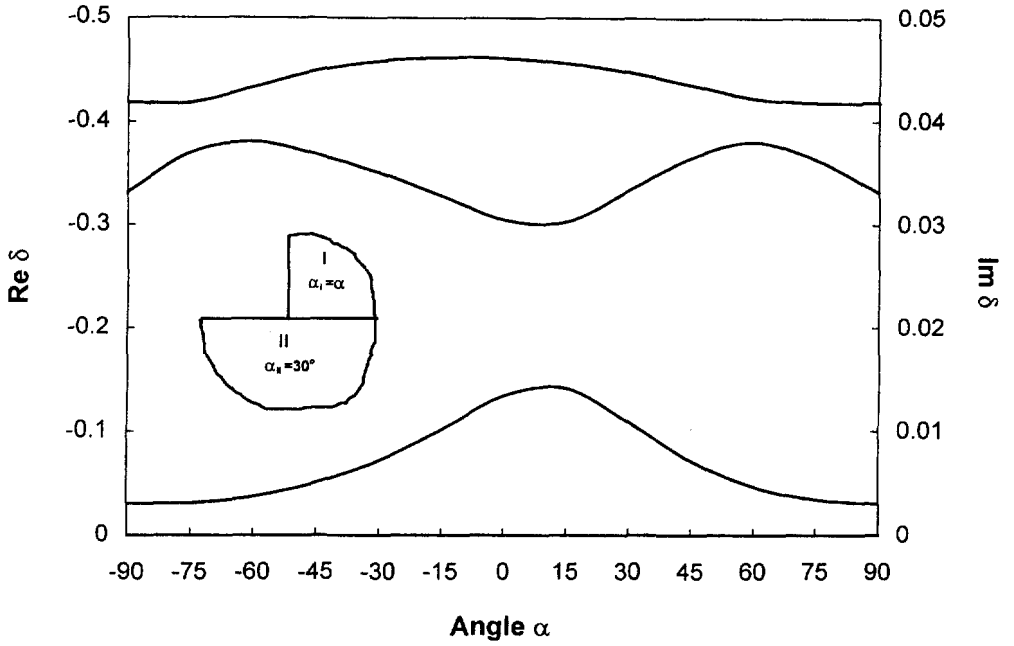

Fig. 6. Order of stress singularity for a two-material wedge with varying the fibre orientation for material I.

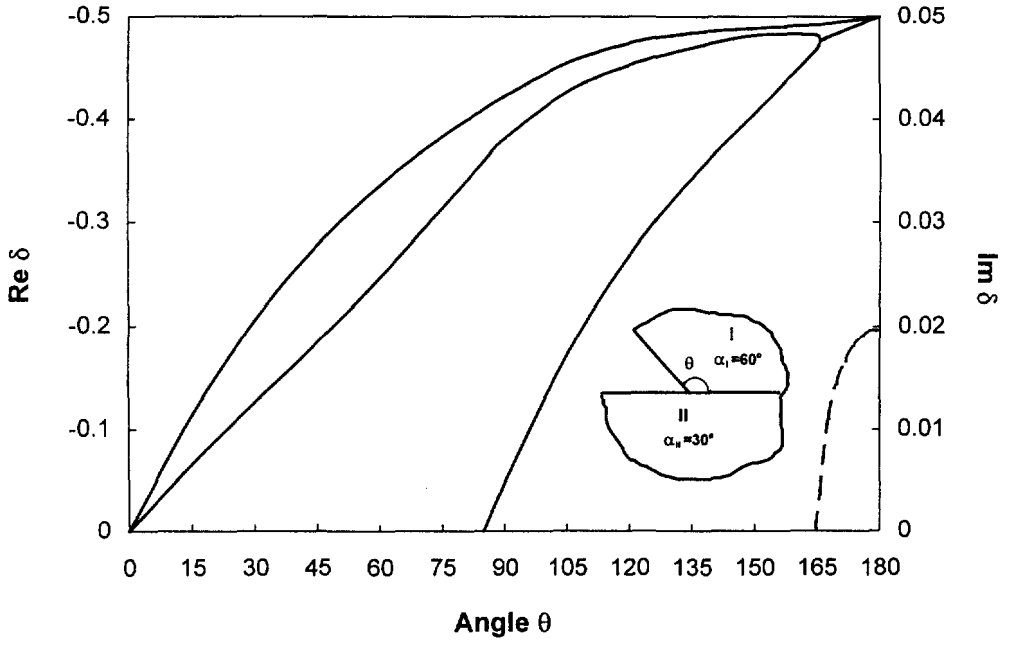

Fig. 7. Order of stress singularity for a two-material wedge with varying the wedge angle for material I.

Fully bonded junctions. The cases of fully bonded two-material junctions are considered as shown in Figs 8 and 9. The fully bonded junction shown in Fig. 9 comprises two materials, i.e., material I with wedge angle 90° and fibre orientation varying from $-90°$ to 90°, and material II with wedge angle 270° and fixed fibre orientation $\alpha_{II} = 45°$. Stress singularities are very low in this case as shown in Fig. 8. Two real roots or a pair of complex conjugate roots exist except that $\delta = 0$ when $\alpha_I = 45°$ since both two materials have the same fibre orientation.

The order of stress singularities varying with the position of a bonded interface θ is investigated as shown in Fig. 9, where the fibre orientations for material I and material II are fixed, i.e., $\alpha_I = -45°$ and $\alpha_{II} = 45°$. The stress singularities become high rapidly as the

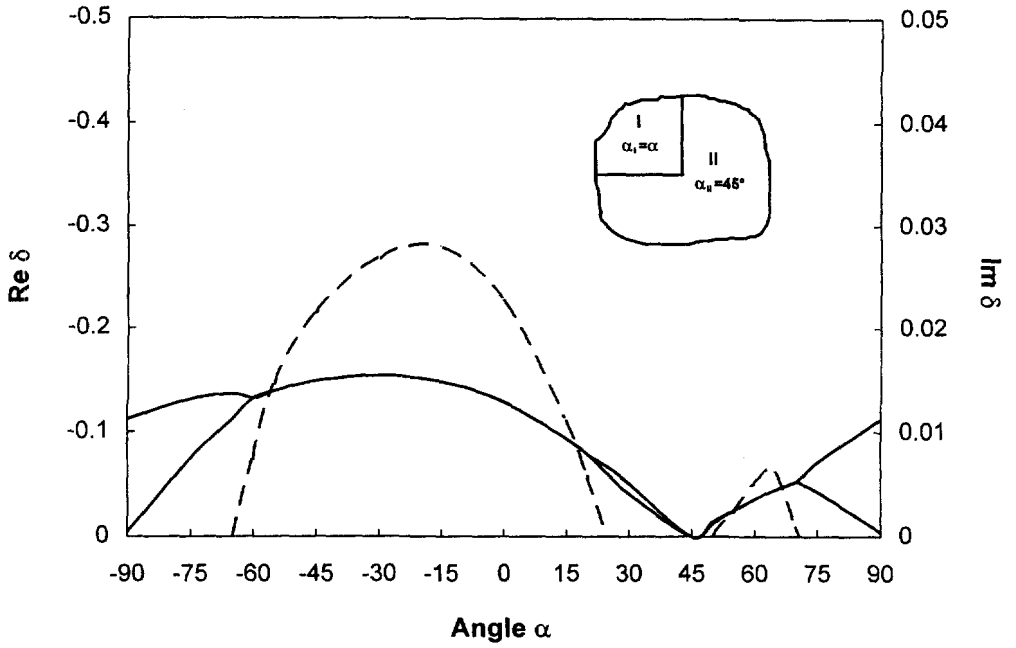

Fig. 8. Order of stress singularity for a fully bonded two-material junction with varying the fibre orientation for material I.

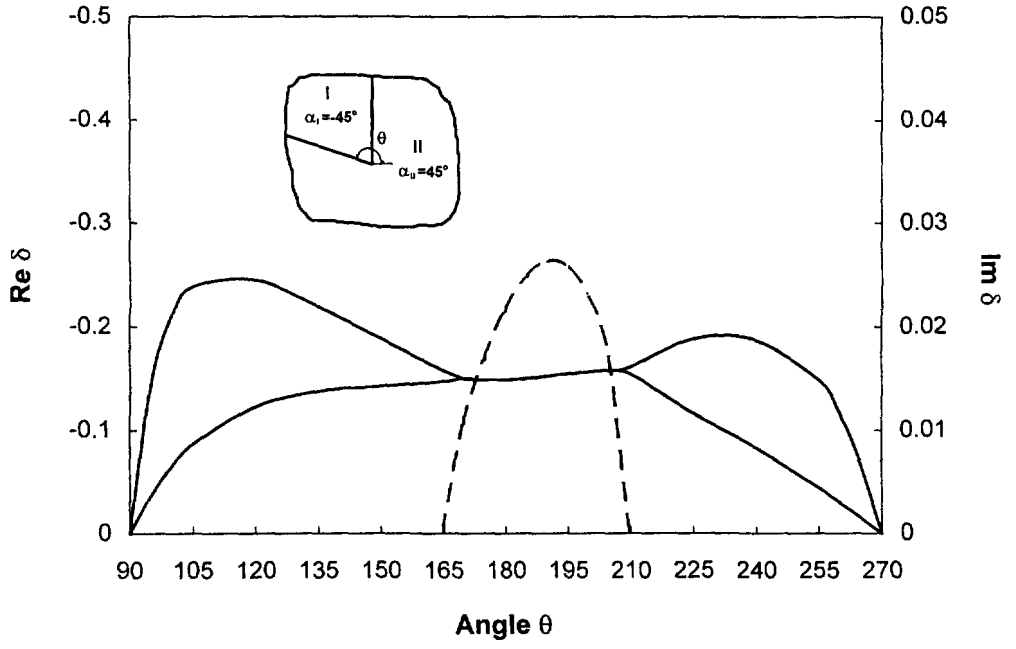

Fig. 9. Order of stress singularity for a fully bonded two-material junction with varying the position of a bonded interface.

interface position θ varies from 90° to 105°, and then reducing slowly until complex roots occur. There are no stress singularities when $\theta = 90°$ in which only material I exists and $\theta = 270°$ in which both wedges for material I and material II are half plane.

Disbonded junctions. The geometric configurations considered in Figs 10 and 11 are similar to those of Figs 8 and 9, respectively, except that one of interface between two materials is disbonded. In these cases, the stress singularities become more severe since a perfectly bonded interface is replaced by a disbond. An "extra" real root corresponding to very low singular stresses is found in both cases in addition to three roots corresponding to

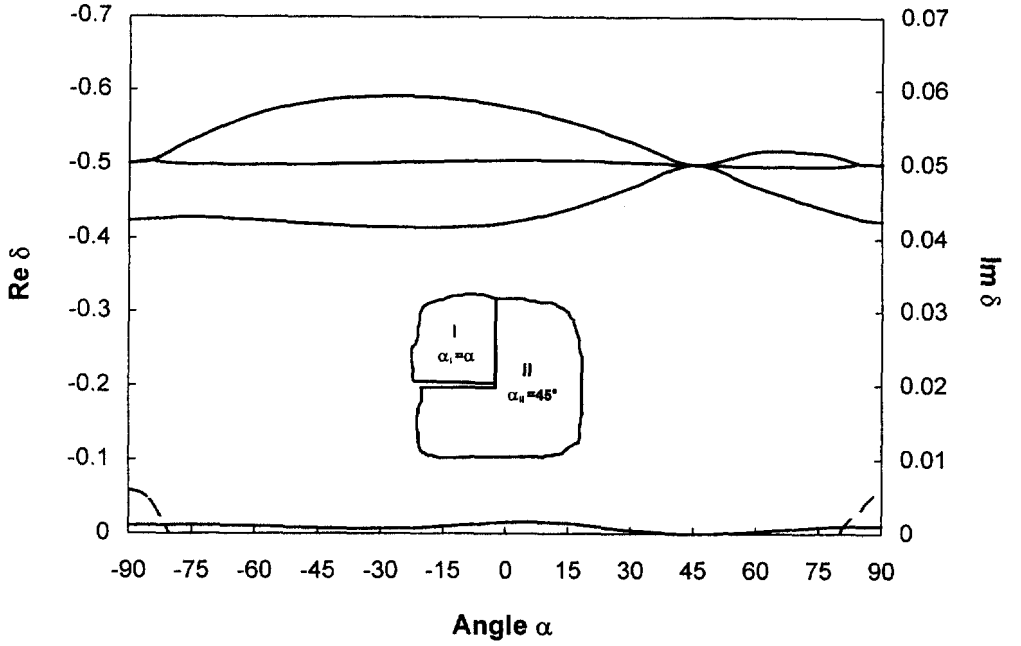

Fig. 10. Order of stress singularity for a disbonded two-material junction with varying the fibre orientation for material I.

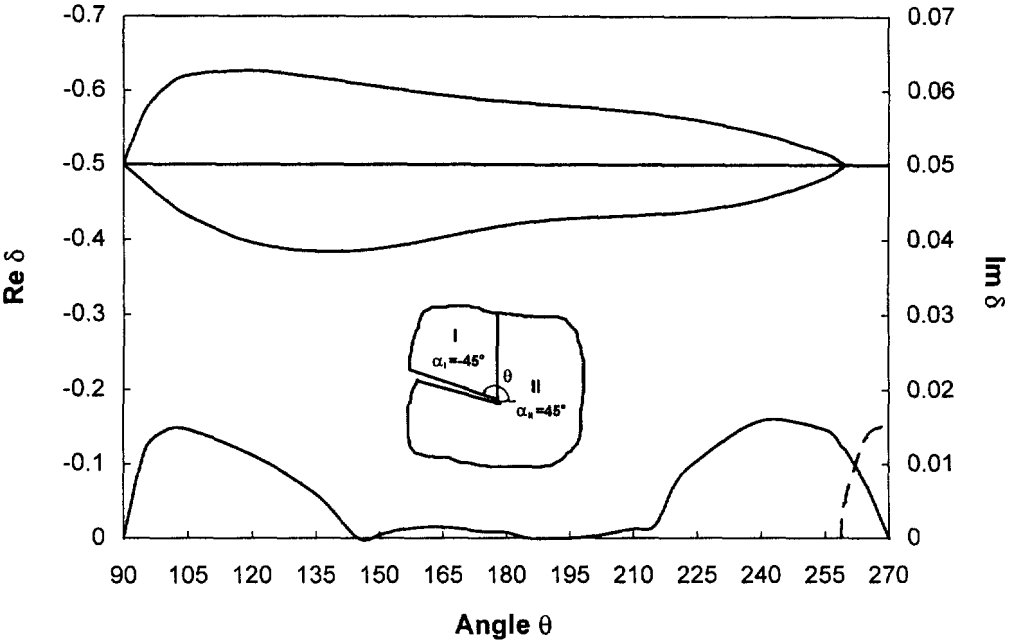

Fig. 11. Order of stress singularity for a disbonded two-material junction with varying the disbond position.

higher singular stresses as shown in Figs 10 and 11. The "extra" real root shown in Fig. 11 also varies with the disbond position θ, reaching the value close to zero when θ is near 180°. It should be noted that $\delta = -1/2$ is a triple root when $\alpha_I = 45°$ in the case of Fig. 10 and when $\theta = 90°$ in case of Fig. 11, and $-1/2$ is a real root and the real parts of a pair of complex conjugate roots when $\theta = 270°$ as shown in Fig. 11, in which the case of Fig. 11 degenerates into the one of interface crack between two anisotropic half plane wedges. Note that the "extra" root vanishes in the degenerated cases mentioned above.

Crack terminating at an interface. Figure 12 shows the case of a crack normal to and ending at an interface between two materials. Here, the fibre orientations for material I and

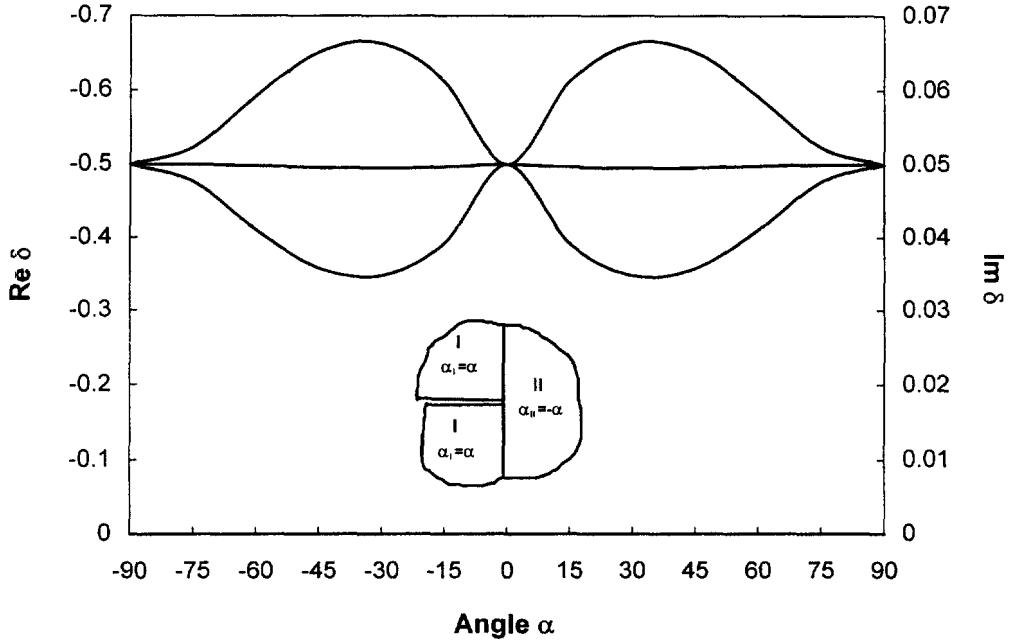

Fig. 12. Order of stress singularity for a crack normal to and ending at an interface between two materials with varying the fibre orientations.

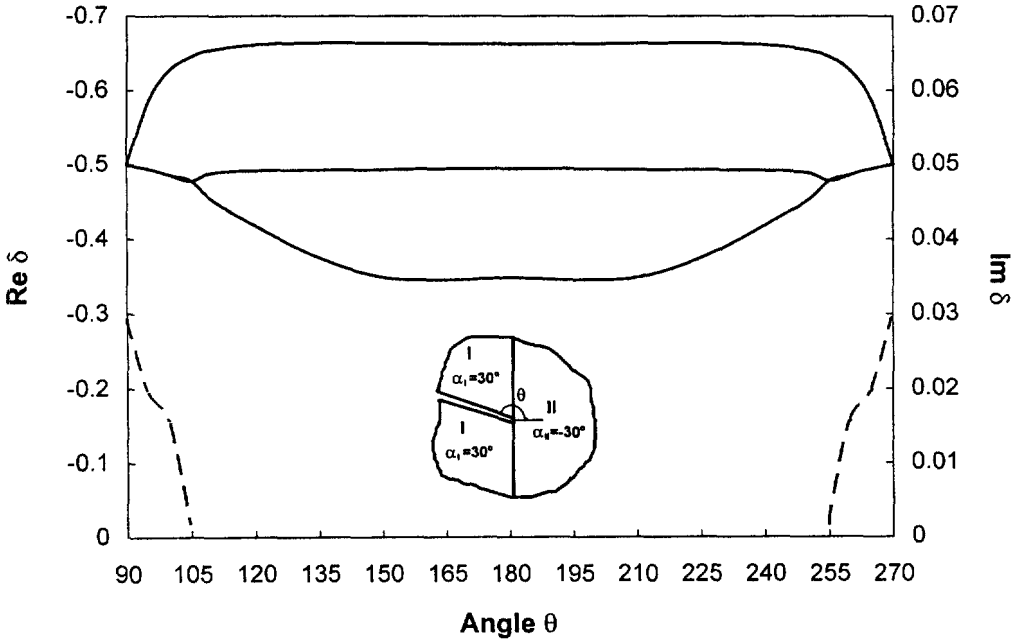

Fig. 13. Order of stress singularity for a crack terminating at an interface between two materials and varying the crack position.

material II are assumed to be $\alpha_I = \alpha$ and $\alpha_{II} = -\alpha$, respectively. A relation between the order of stress singularity δ and the fibre orientation α is given as shown in Fig. 12 with varying α from $-90°$ to $90°$. It can be seen that the values of δ for $(-\alpha/\alpha)$ and $(\alpha/-\alpha)$ are identical, and $\delta = -1/2$ is a triple root when $\alpha = -90°$, $\alpha = 0°$ and $\alpha = 90°$. Three non-equal roots of δ exist for all other combinations of $(\alpha/-\alpha)$.

The results in Fig. 13 are for the case of a crack present in material I and terminating at an interface between two materials. In this case, the fibre orientations for both material I and material II are fixed, i.e., $\alpha_I = 30°$ and $\alpha_{II} = -30°$, while the crack position θ varies from 90° to 270°. Note that the values of roots δ are identical for crack positions on the

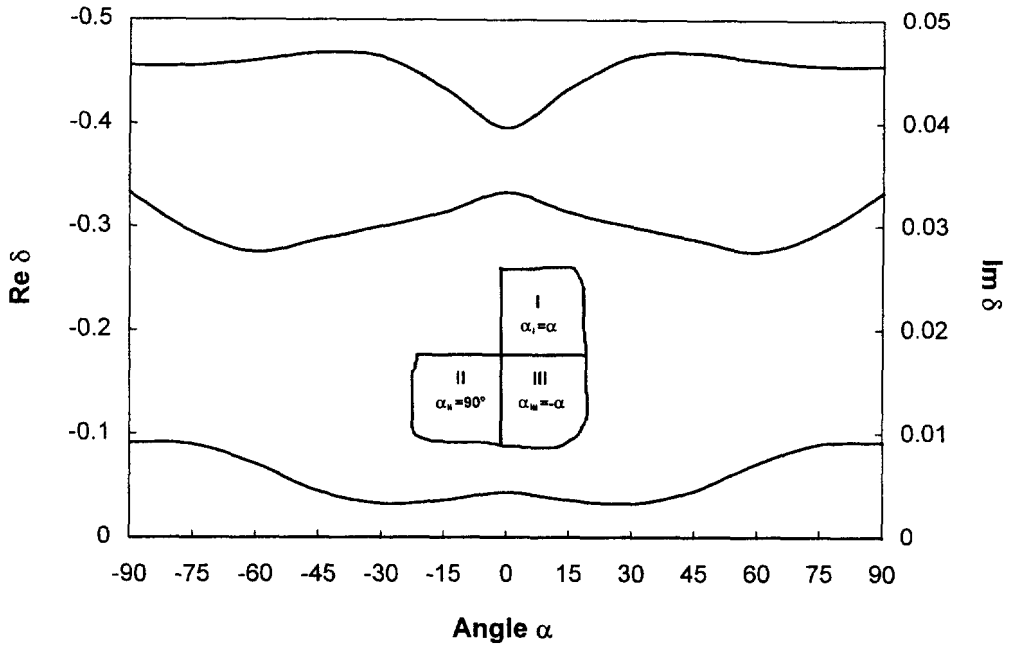

Fig. 14. Order of stress singularity for a three-material wedge with varying the fibre orientations for materials I and III.

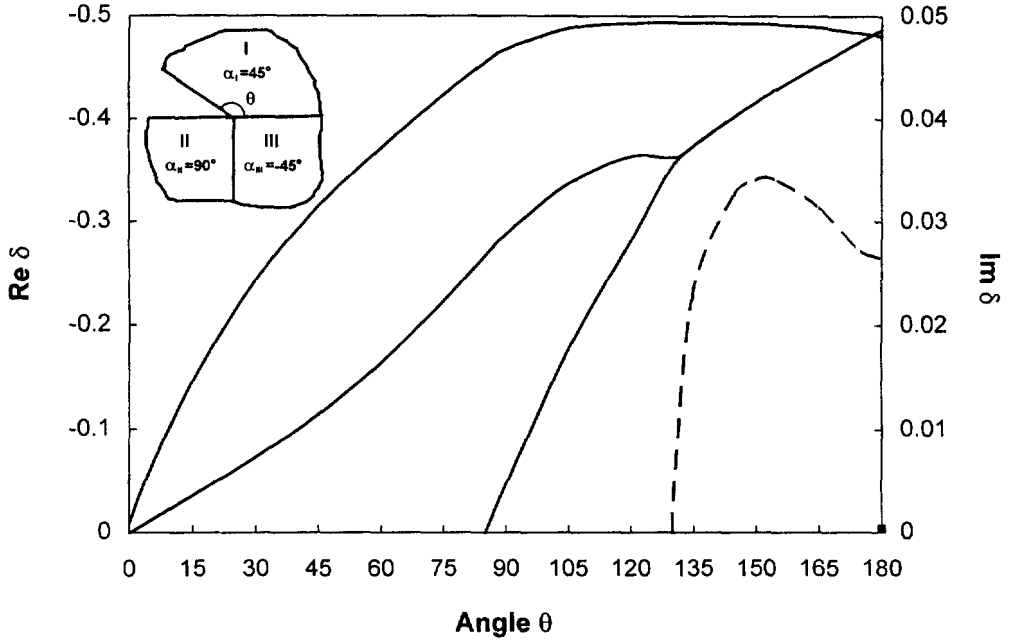

Fig. 15. Order of stress singularity for a three-material wedge with varying the wedge angle for material I.

radical surface θ and the radical surface $360^\circ - \theta$. A real root and a pair of complex conjugate roots exist when a crack is near the bonded interfaces. The case of Fig. 13 degenerates into the one for interface crack between two anisotropic materials when $\theta = 90^\circ$ and $\theta = 270^\circ$.

3.2. *Results for three-material wedges and junctions*

Wedges. The configurations of three-material wedges considered here are shown in Figs 14 and 15. In Fig. 14, results are for a three-material wedge composed of three 90° wedges, where the fibre orientations for material I α_I and material III α_{III} are considered as

the variables with $\alpha_I = \alpha$ and $\alpha_{III} = -\alpha$, while holding $\alpha_{II} = 90°$. It can be seen that the trends are quite different from the ones for two-material wedge as shown in Fig. 6 since the wedge discussed here comprises three different materials. Moreover, the values of roots δ are identical for $(\alpha/90°/-\alpha)$ and $(-\alpha/90°/\alpha)$, where $(\alpha/90°/-\alpha)$ refers to the fibre orientations for materials I, II and III, respectively.

The results shown in Fig. 15 are for a three-material wedge with varying the wedge angle of material I θ from 0° to 180°, while the fibre orientations for all three materials are fixed, i.e., $\alpha_I = 45°$, $\alpha_{II} = 90°$ and $\alpha_{III} = -45°$. The trends are very similar to those observed in Fig. 7 except that the range of complex roots become larger. Note that the values of roots δ are different from those of Fig. 7 when $\theta = 0°$ and $\theta = 180°$, since three different materials are considered here. A real root that represents the order of singular singularity for free-edge problem exists, $\delta = -0.009646$, when $\theta = 0°$. Four roots exist including an "extra" one, $\delta = -0.003902$, when $\theta = 180°$.

Fully bonded junctions. Figures 16 and 17 show the cases of fully bonded three-material junctions. In Fig. 16, a three-material junction composed of two 90° wedges with varying fibre orientations, $\alpha_I = -\alpha$ and $\alpha_{II} = \alpha$, and a half plane with fixed fibre orientation, $\alpha_{III} = 0°$, is considered. All interfaces between materials are assumed to be bounded perfectly. It can be seen that two real roots are very close to zero, which indicates that very low singular stresses exist in this case. No stress singularities exist when $\alpha = -90°$, $\alpha = 0°$ and $\alpha = 90°$, since the case of Fig. 16 is degenerated. Moreover, the values of roots δ for $(-\alpha/\alpha/0°)$ and $(\alpha/-\alpha/0°)$ are identical due to symmetric fibre orientations.

The case considered in Fig. 17 is for a three-material junction composed of three wedges with varying the position of the bonded interface between material I and material II θ from 90° to 270°. The fibre orientations for all three materials are fixed, i.e., $\alpha_I = -45°$, $\alpha_{II} = 45°$ and $\alpha_{III} = 0°$. Only one real root exists except when the bonded interface position θ is near 180°. It can be seen from the results for a three-material fully bonded junction only low singular stresses exist and the values of roots δ are real. Since the fibre orientations for material I and material II are symmetric, the values of roots δ are identical for the bonded interface positions on the radical surface θ and the radical surface $360° - \theta$.

Disbonded junctions. Several cases of disbonded three-material junctions are now considered, and results for these cases are presented in Figs 18–21. Here, one of the

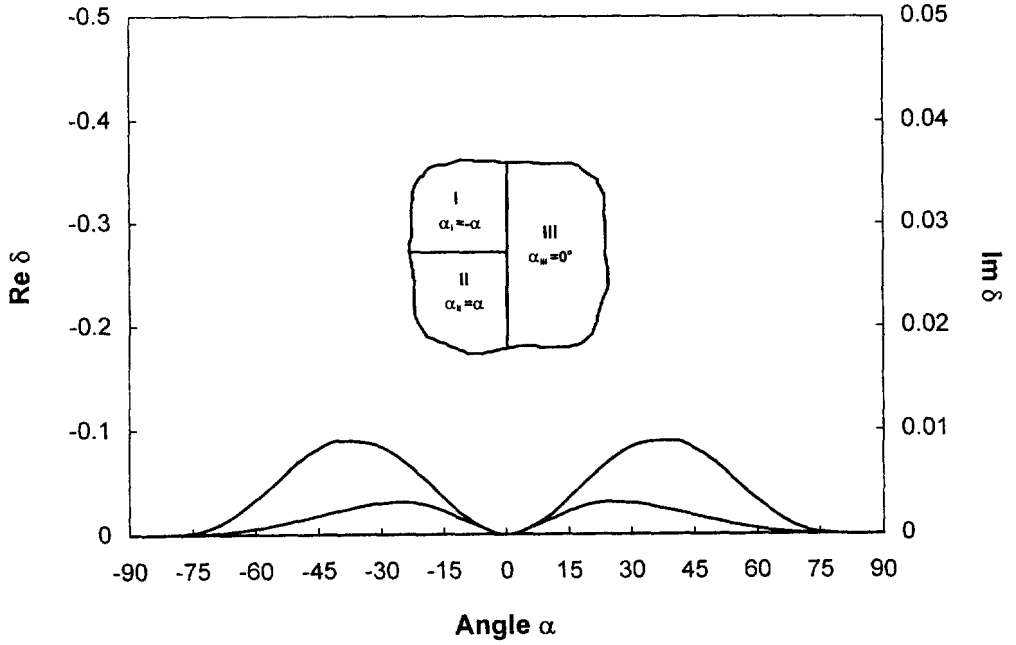

Fig. 16. Order of stress singularity for a fully bonded three-material junction with varying the fibre orientations for materials I and II.

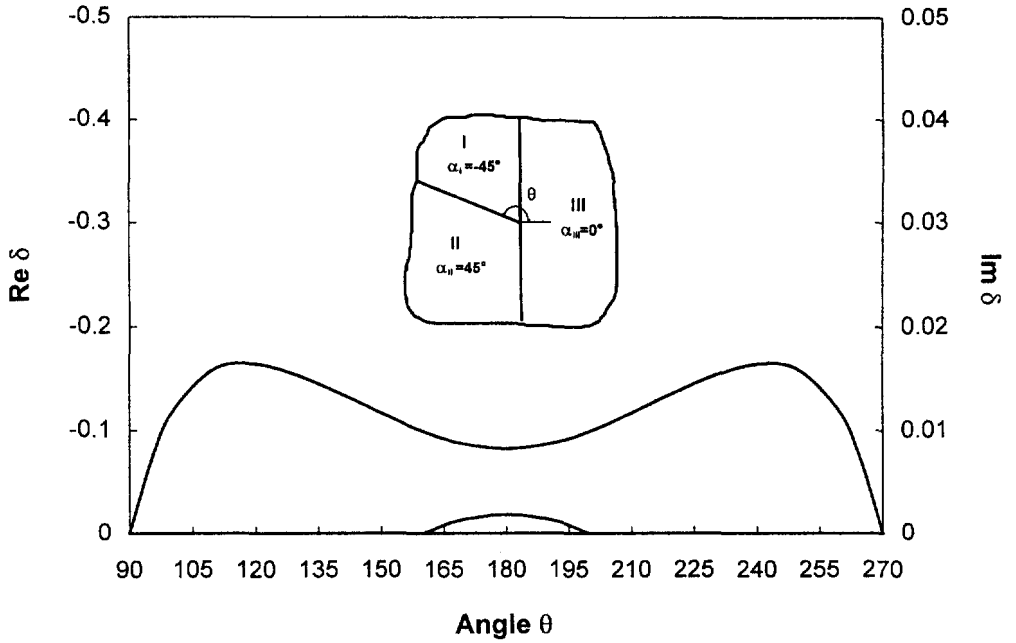

Fig. 17. Order of stress singularity for a fully bonded three-material junction with varying the position of a bonded interface between materials I and II.

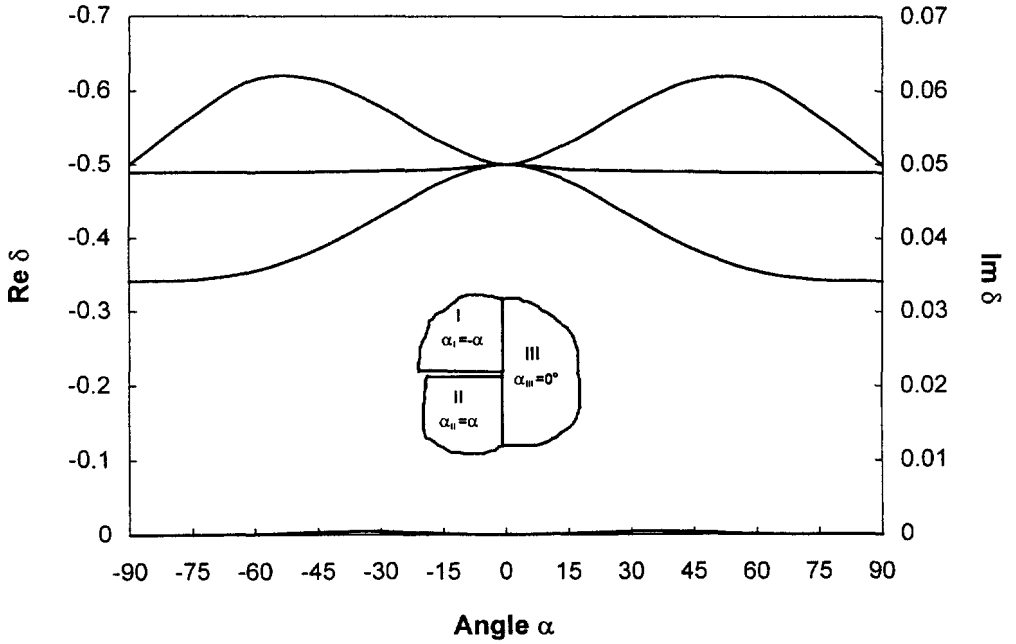

Fig. 18. Order of stress singularity for a disbonded three-material junction with a disbond along the interface between materials I and II, and varying the fibre orientations for materials I and II.

interfaces between materials is assumed to be disbonded and other two interfaces bonded perfectly. In order to show the effect of the positions of disbond on stress singularities, different disbond positions are discussed.

Figure 18 shows the case of a disbonded three-material junction composed of a half plane with $\alpha_{III} = 0°$ and two 90° wedges with $\alpha_I = -\alpha$ and $\alpha_{II} = \alpha$. A disbond is introduced along the interface between material I and material II. A relation between the order of stress singularity δ and the fibre orientation α is investigated with varying α from $-90°$ to 90°. Four real roots exist including an "extra" root corresponding to very low singular stresses. The values of roots δ for $(-\alpha/\alpha/0°)$ and $(\alpha/-\alpha/0°)$ are identical due to symmetric

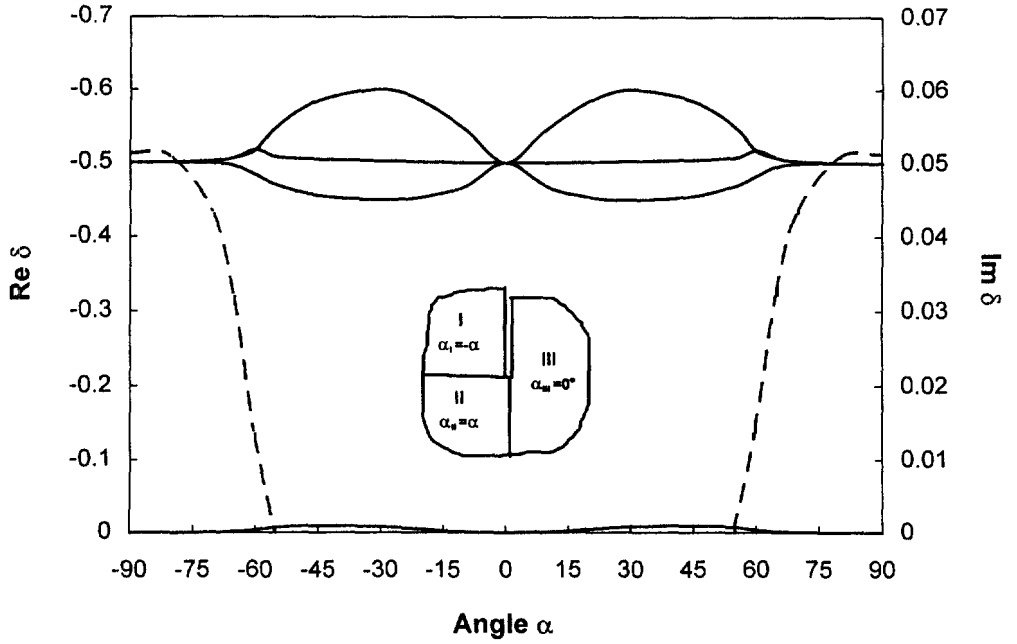

Fig. 19. Order of stress singularity for a disbonded three-material junction with a disbond along the interface between materials I and III, and varying the fibre orientations for materials I and II.

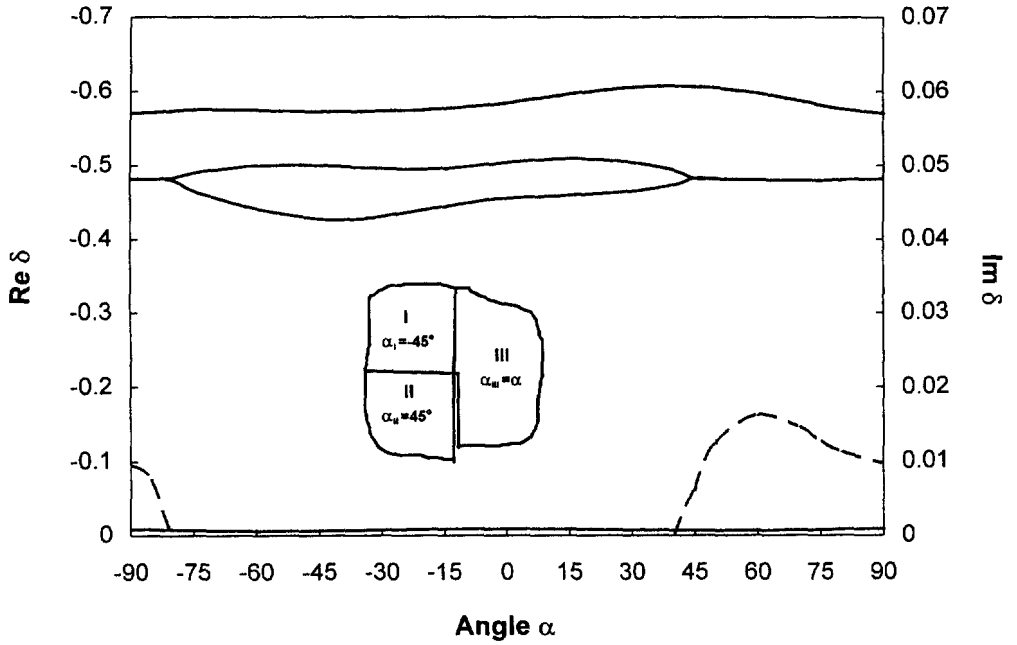

Fig. 20. Order of stress singularity for a disbonded three-material junction with a disbond along the interface between materials II and III, and varying the fibre orientations for material III.

fibre orientations. Note that $\delta = -1/2$ is a triple root when $\alpha = 0°$, but $\delta = -1/2$ is only one of three real roots when $\alpha = -90°$ and $\alpha = 90°$. In these degenerated cases, the "extra" root vanishes.

The results shown in Fig. 19 are for a disbonded three-material junction with a disbond along the interface between material I and material III. The fibre orientations for material I and material II are considered as the variables with $\alpha_I = -\alpha$ and $\alpha_{II} = \alpha$, while holding $\alpha_{III} = 0°$. Here, complex roots are found, and an "extra" root is also observed. The values of roots δ are identical for $(-\alpha/\alpha/0°)$ and $(\alpha/-\alpha/0°)$. Note that the case of Fig. 19 degenerates into the one of an interface crack between two anisotropic materials when $\alpha = -90°$ and $\alpha = 90°$, and $\delta = -1/2$ is a triple root when $\alpha = 0°$.

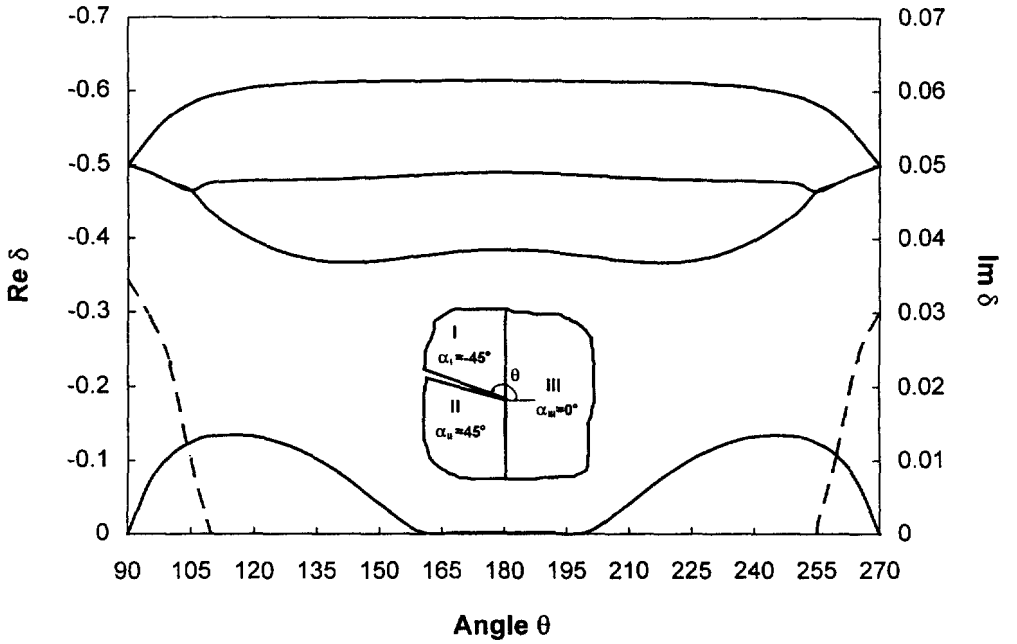

Fig. 21. Order of stress singularity for a disbonded three-material junction with a disbond along the interface between materials I and II, and varying the disbond position.

In Fig. 20, the configuration is similar to those of Figs 18 and 19, but a disbond is present along the interface between material II and material III. Here, the fibre orientations for material I and material II are fixed, $\alpha_I = -45^\circ$ and $\alpha_{II} = 45^\circ$, while $\alpha_{III} = \alpha$ varying α from -90° to 90°. It is found that the values of roots δ are identical for the case of Fig. 19 and the case of Fig. 20 when fibre orientations for both cases are $(-\alpha/\alpha/0^\circ)$. Also, from the results shown in Fig. 20, it can be found that there are four roots including an "extra" root corresponding to very low singular stresses.

The results in Fig. 21 show how the order of stress singularity varies with the disbond position θ ranging from 90° to 270°. The disbonded junction considered here comprises three different materials with fixed fibre orientations, i.e., $\alpha_I = -45^\circ$, $\alpha_{II} = 45^\circ$ and $\alpha_{III} = 0^\circ$. The trends are similar to those observed in Fig. 13 except that an "extra" root corresponding to lower singular stresses exists. The "extra" root varies with the disbond position, reaching the value of a real root $\delta = -0.135433$ when $\theta = 115^\circ$, and then reducing to the value close to zero when θ is near 180°. Note that the degenerated cases can be considered as an interface crack between two materials when $\theta = 90^\circ$ and $\theta = 270^\circ$, where the "extra" root vanishes.

From the results shown in Figs 18–21, it can be seen that stress singularities become obviously high compared with the fully bonded cases as shown in Figs 16 and 17. However, the values of roots δ corresponding to the highest singular stresses for each case shown in Figs 18–20 are close to each other, and usually less than $-1/2$. The values of roots δ corresponding to the highest singular stresses shown in Fig. 21 keep almost the same within large range of the crack position from 90° to 270°. Moreover, it can be found that usually there are four roots including an "extra" one in all cases as shown in Figs 18–21.

4. CONCLUSIONS

The order of the stress singularities for anisotropic two- and three-material wedges and junctions that are either perfectly bonded at their interfaces or a disbond along one of interfaces is investigated. The results for variations of the order of stress singularity with geometric properties, e.g., the wedge angle, the bonded interface position, the disbond position and the crack position, and material properties, e.g., the fibre orientation, have been provided. The significant changes of stress singularities will take place when a fully

bonded interface becomes a disbond along the interface for the cases of anisotropic two and three-material junctions.

An "extra" root that corresponds to very low singular stresses is found for the cases of disbonded two and three-material junctions (see Figs 10–11, 18–21). The results then provide a way to obtain an accurate elastic stress analysis of the problems of anisotropic multi-material wedges and junctions since all of the roots must be taken into account.

The results presented here will be useful for selecting wedge angle and material combinations for anisotropic material wedges and junctions in order to reduce the stress concentration, and assist the design against the failure of composite materials and structures. It should be pointed out that the present developed approach can be further extended to deal with problems such as deformation fields and singular stress fields around the singular point, more general orientations for fibres as well.

REFERENCES

Delale, F. (1984) Stress singularities in bonded anisotropic materials. *International Journal of Solids and Structures* **20,** 31–40.

Huang, T. F. and Chen, W. H. (1994) On the free-edge stress singularity of general composite laminates under uniform axial strain. *International Journal of Solids and Structures* **31,** 3139–3151.

Inoue, T. and Koguchi, H. (1996) Influence of the intermediate material on the order of stress singularity in three-phase bonded structure. *International Journal of Solids and Structures* **33,** 399–417.

Lekhnitskii, S. G. (1963) *Theory of Elasticity of an Anisotropic Body*. Holden-Day, San Francisco.

Muller, D. E. (1956) A method for solving algebraic equations using an automatic computer. *Mathematical Tables and Computations* **10,** 208–215.

Pageau, S. S. and Biggers, S. B. Jr. (1994) The order of stress singularities for bonded and disbonded three-material junctions. *International Journal of Solids and Structures* **31,** 2979–2997.

Pageau, S. S., Joseph, P. F. and Biggers, S. B. Jr. (1995) A finite element analysis of the singular stress fields in anisotropic materials loaded in antiplane shear. *International Journal for Numerical Methods in Engineering* **38,** 81–97.

Pageau, S. S. and Biggers, S. B. Jr. (1996) A finite element approach to three-dimensional singular stress states in anisotropic multi-material wedges and junctions. *International Journal of Solids and Structures* **33,** 33–47.

Stroh, A. N. (1962) Steady state problems in anisotropic elasticity. *Journal of Mathematical Physics* **41,** 77–103.

Ting, T. C. T. and Chou, S. C. (1981) Edge singularities in anisotropic composites. *International Journal of Solids and Structures* **17,** 1057–1068.

Ting, T. C. T. and Hoang, P. H. (1984) Singularities at the tip of a crack normal to the interface of an anisotropic layered composite. *International Journal of Solids and Structures* **20,** 439–454.

Ting, T. C. T. (1986) Explicit solution and invariance of the singularities at an interface crack in anisotropic composites. *International Journal of Solids and Structures* **22,** 965–983.

Wang, A. S. D. and Crossman, F. W. (1977) Some new results on edge effects in symmetric composite laminates. *Journal of Composite Materials* **11,** 92–106.

Wang, S. S. and Choi, I. (1982) Boundary-layer effects in composite laminates. Part 1 : free-edge stress singularities. *Journal of Applied Mechanics* **49,** 541–548.

Yeh, J. R. and Tadjbakhsh, I. G. (1986) Stress singularity in composite laminates by finite element method. *Journal of Composite Materials* **20,** 347–364.

Zwiers, R. I., Ting, T. C. T. and Spilker, R. L. (1982) On the logarithmic singularity of free-edge stress in laminated composites under uniform extension. *Journal of Applied Mechanics* **49,** 561–569.